Journal of Photochemistry & Photobiology, B: Biology 259 (2024) 113019

Contents lists available at ScienceDirect

Journal of Photochemistry & Photobiology, B: Biology

journal homepage: www.elsevier.com/locate/jphotobiol

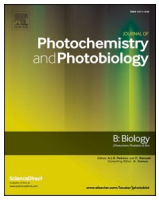

The effect of near-infrared Photobiomodulation therapy on the ion content of 50B11 sensory neurons measured through XRF analysis

Luisa Zupin [a,*], Alessandra Gianoncelli [b], Fulvio Celsi [a,*], Valentina Bonanni [b], George Kourousias [b], Pietro Parisse [b,c], Murielle Salomé [d], Sergio Crovella [e], Egidio Barbi [a,f], Giuseppe Ricci [a,f], Lorella Pascolo [a]

[a] Institute for Maternal and Child Health, IRCCS Burlo Garofolo, 34137 Trieste, Italy
[b] Elettra Sincrotrone Trieste, Basovizza, 34149, Trieste, Italy
[c] CNR-IOM, Basovizza, 34149 Trieste, Italy
[d] ESRF, European Synchrotron Radiation Facility, Cedex 9, F-38043 Grenoble, France
[e] Laboratory of Animal Research (LARC), Qatar University, 2713, Doha, Qatar
[f] Department of Medical, Surgical and Health Science, University of Trieste, 34100, Trieste, Italy

ARTICLE INFO

Keywords:
Photobiomodulation therapy
Ion content
Sensory neurons
XRF analysis
AFM

ABSTRACT

Photobiomodulation therapy (PBMT) is a form of treatment commonly used for routine clinical applications, such as wound healing of the skin and reduction of inflammation. Additionally, PBMT has been explored for its potential in pain relief.

In this work, we investigated the effect of PBMT on ion content within the 50B11 sensory neurons cell line in vitro using X-Ray fluorescence (XRF) and atomic force microscope (AFM) analysis.

Two irradiation protocols were selected utilizing near-infrared laser lights at 800 and 970 nm, with cell fixation immediately following irradiation.

Results showed a decrease in Calcium content after irradiation with both protocols, and with lidocaine, used as an analgesic control. Furthermore, a reduction in Potassium content was observed, particularly evident when normalized to cellular volume.

These findings provide valuable insights into the molecular impact of PBMT within 50B11 sensory neurons under normal conditions. Such understanding may contribute to the wider adoption of PBMT as a therapeutic approach.

1. Introduction

Photobiomodulation therapy (PBMT) is a widely employed treatment for routine clinical applications, ranging from wound healing of the skin and the mucosae tissues to reducing inflammation. Moreover, PBMT was previously exploited for pain relief. However, new applications in the neuroscience field have arisen, such as treating the central nervous system for neurodegenerative diseases and cognitive impairment, but also for traumatic damage of the peripheral nervous system [1]. The therapeutic effects of PBMT are also applied in the pediatric field; indeed, different conditions can benefit from the topical application of laser light for wound healing and pain therapy. Oral mucositis [2], recurrent aphthous stomatitis [3], injection pain during local anaesthesia [4], can all improve after PBMT.

Near-infrared (NIR) and red wavelengths have been revealed as the most potent inducing analgesia. Indeed, several studies conducted in experimental *in vitro* [5] models and clinically on human patients highlighted the beneficial effect of 630, 800–830 and 900 nm wavelengths [5].

The transcutaneous and transmucosal delivery of photons to nerves may lead to the inhibition of the noxious signalling transmission, thus resulting in reduced painful sensations. Electrophysiological studies on peripheral nerves revealed that PBMT slowed the conduction velocity, reduced the amplitude of compound action potentials in humans, and

Abbreviations: AFM, atomic force microscope; DRG, dorsal root ganglion; NIR, Near-infrared; PBMT, Photobiomodulation therapy; TRP, transient receptor potential; XRF, X-Ray fluorescence.

* Corresponding authors.
E-mail addresses: luisa.zupin@burlo.trieste.it (L. Zupin), fulvio.celsi@burlo.trieste.it (F. Celsi).

https://doi.org/10.1016/j.jphotobiol.2024.113019
Received 10 May 2024; Received in revised form 19 August 2024; Accepted 22 August 2024
Available online 23 August 2024

decremented the somatosensory evoked potentials in animal models [6]. The suppression of the pro-inflammatory bradykinin activity, the downregulation of B1 and B2 kinin receptors and the decrement of substance P (a nociceptive mediator) level were also determined after PBMT in animal studies [6]. Nevertheless, a precise description of the molecular mechanisms based on these observed effects must still be defined. Different cellular acceptors of photons have been proposed, including the mitochondria, specifically the cytochrome C oxidase, the final enzyme (complex IV) of the mitochondrial electron transfer chain, which is claimed to be the primary photoreceptors of PBMT [7], or ion channels that can be light sensitive, such as transient receptor potential (TRP) [8].

We have previously demonstrated that pre-irradiation of dorsal root ganglion (DRG) murine sensory neurons [9] and 50B11 immortalized rat sensory neurons [10] with NIR PBMT reduces the flow of calcium-induced by capsaicin, a known ligand of the TRP vanilloid 1 channel (TRPV1).

Another possible mechanism of action could be related to the induction of beta-tubulin varicosities in the neurites, blocking fast axonal flow and anterograde transport of mitochondria. These events reduce the bioavailability of ATP which is fundamental to generating action potential by NA+/K+ ATPase [11]. Accordingly with these results, we previously demonstrated that in DRG neurons NIR PBMT at 800 and 970 nm reduced the ATP content but not in 50B11 cells [10,9], while the 905 nm wavelength could decrease it in 50B11 cells [12].

NIR light also influences protein kinases A and C (PKA and PKC), whose pathways are usually involved in the decrement of the nociception activation threshold by phosphorylating TRPV1. Therefore, the blockade of PKA and PKC by PBMT reduces the nociceptive response in animal pain models [13].

It has been reported that PBMT at 830 nm reduces the mitochondrial membrane potential (MMP) in rat DRG neurons. However, supplementing sodium channel blockers abolished the depolarization, suggesting a direct effect on sodium channels [14]. MMP depolarization provoked by PBMT has also been involved in Ca^{2+} release from intracellular stores, in neural cells, suggesting again a direct effect on mitochondria metabolism and Ca^{2+} homeostasis [15].

In the present work, the immortalized 50B11 cell line was employed as a model of sensory neurons isolated from rat dorsal root ganglion, which develops neuronal features and expresses markers of sensory neurons upon differentiation with forskolin [16].

The cells were irradiated with two protocols of NIR PBMT that were chosen based on our previous experience with this cell line [10], employing 800 and 970 nm wavelengths. Since PBMT may have a direct impact on several proteins involved in the transport of ions both at the level of the membrane [17] and of mitochondria [15], the chemical elements modifications inside the cells were investigated by synchrotron X-ray fluorescence microscopy. This technique was non-destructive and allowed quantifying the element's content and contemporaneously mapping the element's distribution inside the cells [18,19,20], giving a still picture of the PBMT effect, locked immediately after irradiation.

Based on these considerations, our study aims to expand knowledge in the field of analgesia induced by PBMT, by comparing the chemical elements content and distribution of laser-treated neurons with untreated control cells and lidocaine-exposed neurons.

2. Materials and Methods

2.1. 50B11 Cell Culture

50B11 sensory neurons were maintained in Neurobasal medium (21,103,049, Life Technologies, Thermo Fisher Scientific, Waltham, MA, USA) with 2 % B27 supplement (Life Technologies), 10 % fetal bovine serum (Euroclone, Pero, Milan, Italy), 0.22 % glucose (Merck, Saint Louis, Missouri, USA), 0.2 mM glutamine (Euroclone) and 100 U/mL Penicillin/Streptomycin (Euroclone).

The cells were seeded on Si_3N_4 windows (Silson) in 12 multi-well plates at a cellular density of 10.000 cells/well in Neurobasal medium without phenol red (12,348,017, Life Technologies) and differentiated in forskolin (75 μM, F6886, Merck) for 24 h.

At the end of the experimental setting, the cells were irradiated with a class IV diode laser (class IV, K-Laser Cube series, K-Laser d.o.o., Sežana, Slovenia) with two protocols: 800 and 970 nm wavelengths, power 0.6 W, irradiance 0.3 W/cm^2, total delivered energy 3 J; in pulsed modality at 5 Hz with 50 % duty cycle. The protocols were selected based on our previous experience with PBMT on this cell line and employing the pulse mode of irradiation [10]. Immediately after PBMT, the cells were fixed in paraformaldehyde 4 % in phosphate buffer saline (PBS) at room temperature for 20′, then they were washed twice in PBS, twice in distilled water, air dried and maintained at room temperature until XRF analysis. Photobiomodulation induced immediate pain relief [21], so considering that the 50B11 cells are sensory neurons, we decided to select and analyse only the immediate effect of PBMT.

As a control for the analgesic effect, lidocaine treatment (a known anaesthetic drug) was employed. Briefly, the cells were treated for 5′ with lidocaine 50 or 100 μM, washed in PBS and fixed as described above.

2.2. XRF Analysis

XRF analyses were performed at two different synchrotron facilities under two complementary set-ups.

At the ID21 beamline [22,23] of the European Synchrotron Radiation Facility (ESRF, Grenoble, France), a 7.3 keV monochromatic X-ray beam was focused onto the sample using Kirkpatrick-Baez mirrors (KB) with a spot size of 0.91 μm × 0.29 μm (H x V) and with a photon flux of 1.094e11 photon/s/Si(111) bandwidth. The sample was raster-scanned across the microprobe, forming an incident angle of 45 degrees concerning the sample plane, while the XRF detector was located at 90 degrees from the incident beam. The acquisition time was typically 100 ms/pixel with a step size of 500 nm. Key chemical elements like Ca, K, S and P can be detected in the selected incident energy.

Low Energy XRF (LEXRF) analyses were performed at the TwinMic beamline at Elettra Sincrotrone Trieste (Trieste, Italy) [24]. For the present experiment, the TwinMic microscope was operated in scanning transmission mode (STXM), where the beam is focused on the sample through a zone plate diffractive optics (600 μm in diameter with 50 nm outermost zone width) delivering a micrometric or sub-micrometric probe size. While the sample is raster-scanned perpendicularly to the incoming monochromatized beam, a fast readout CCD camera collects the transmitted X-rays [25], and an 8 Silicon Drift Detectors-based XRF system acquires the emitted fluorescence photons [26]. The obtained absorption and phase contrast images outline the morphological features of the sample at sub-micrometre length scales. Moreover, the simultaneous detection of the low-energy XRF correlates the elemental distribution to the morphology. For the described experiments, a photon energy of 1.5 keV was used to excite and get optimal emission conditions for the elements of significant interest, namely Mg, Na and other lighter elements, in particular O. The spot size was set to 800 nm; the dwell time for XRF mapping was 6 s per pixel while for STXM imaging was 50 ms per pixel.

All elemental distributions were obtained by processing, deconvolving and fitting the XRF spectra with the PyMCA software [27].

The histograms in Figs. 2 and 5 were obtained by calculating the average XRF intensity of specific chemical elements inside each analyzed cell. The histograms of Fig. 7 are additionally normalized for the corresponding cells' volumes calculated from the Atomic Force Microscopy (AFM) measurements. For each condition (untreated and treated cells), at least 10 cells were considered.

2.3. AFM Analysis

The AFM measurements were performed at the CNR-IOM AFM Asylum laboratory. Suitable cells were selected through visible light microscopy and mapped with AFM-microscopy before XRF analysis. In this way, we avoided any possible artefacts caused by radiation damage induced by soft X-rays. AFM micrographs were acquired in contact and AC modes in the air with an MFP-3D Bio (Asylum Research/Oxford Instruments) instrument. For the acquisition of images in contact or AC mode, we used soft and medium soft cantilevers (Mikromasch CSC38, radius of curvature <10 nm, spring constant 0.006–0.03 N/m for contact mode, Mikromasch NSC 36, radius of curvature <10 nm, spring constant 0.6–2 N/m for AC mode) adjusting the scanning rate in the range 0.2–0.75 Hz, depending on the imaging conditions and a 80–160 nm pixel resolution. Images were analyzed with Gwyddion software [28]; volume extraction was carried out by flattening the image to remove he background, selecting the cells by a height-threshold-based mask, and measuring the minimum basis volume of the single cells.

2.4. Statistical Analysis

Statistical analysis was performed in R software [29] using ANOVA and Dunnett multiple comparison tests.

3. Results

Our study utilized XRF analysis to investigate ion content and elemental distribution inside cells immediately after PBMT treatments to clarify the treatment's effect on neurons.

The employed protocols of PBMT were carefully selected based on our previous tests on 50B11 sensory neurons. In our early work on this cell line, we examined various parameters after irradiation using 12 different fluence and wavelength protocols. The two protocols utilized in this study were chosen for their ability to modify multiple features inside the cell, each with its peculiarity and differences (see reference [10] or details).

Both protocols effectively increased oxidative stress and mitochondrial membrane potential: the 800 nm protocol demonstrated the ability to enhance ATP content and superoxide anion production, while the 970 nm protocol showed a capability to reduce calcium flow after capsaicin. Although the subsequent XRF analysis did not allow us to replicate the same test on the cells, cell morphology and viability were carefully examined at the optical microscope.

After cell fixation, the XRF measurements were performed in the same experimental conditions for each treatment and for the control samples. Thus, we directly compared the elemental content among the different treatment conditions. First, cells were mapped at the ID21 beamline to evaluate the elemental distribution of P, S, K and Ca along the cells at submicrometric resolution. Fig. 1 depicts a representative set of cells for the four distinct conditions (control cells, cells exposed to 800 nm and 970 nm wavelength laser, and lidocaine).

Then, element content was compared among the different conditions by selecting single cells, excluding the support. Due to the high number of analyzed cells, this was done systematically and automatized by considering only the areas where P levels were between 15 % and 100 %, thus excluding the sample support and possible cellular residuals, as displayed in Fig. 2. Moreover, for maps containing more than one cell, we ensured that every single cell was evaluated separately by generating multiple single masks. For instance, for the cells of Fig. 1b exposed to 800 nm, two masks were generated (Fig. 2b and c) from the corresponding P XRF map (Fig. 2a) to ensure single-cell analysis. Panel d in Fig. 2 shows the trend of the average P, S, K and Ca content for the four different conditions.

A decrease in Ca content was observed after the treatment with both

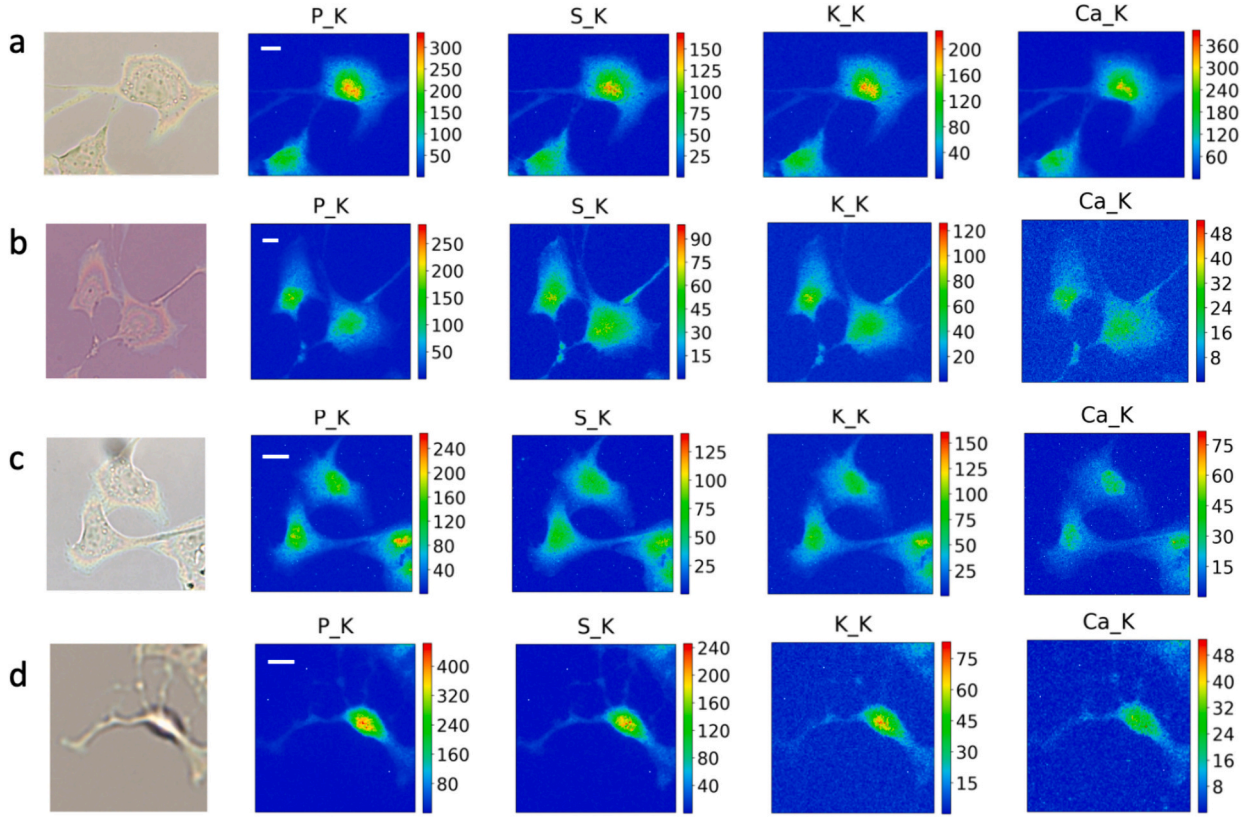

Fig. 1. XRF maps of P, S, K and Ca of control neurons (a) and 800 nm laser (b), 970 nm laser (c) and lidocaine (d) exposed neurons, depicted together with the corresponding visible light images. The XRF maps were acquired at 7.3 keV with a stepsize of 0.5 μm and an acquisition time of 0.1 s/pixel. Scale bars are 10 μm.

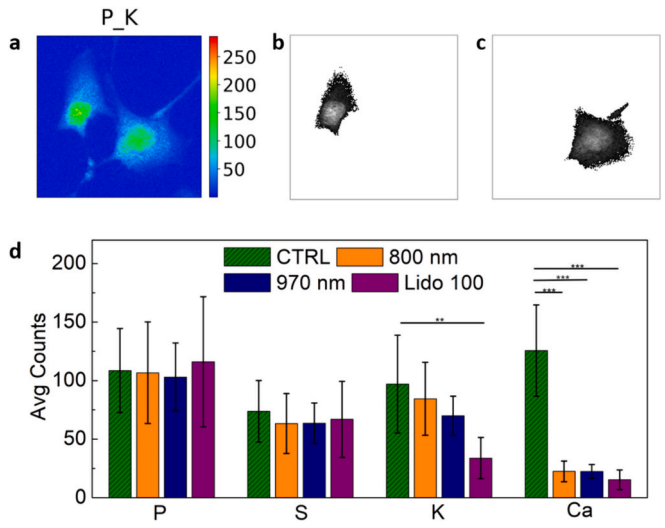

Fig. 2. (a) P XRF map of the neurons exposed to 800 nm laser present in Fig. 1b. (b and c) Masks were extracted from the P XRF map (a) by selecting only pixels with P content higher than 15 % of the maximum level. Each mask must represent a single cell. (d) Bar plots showing the average P, S, K and Ca levels extracted from the corresponding P, S, K and Ca maps for each mapped cell by using the generated masks for control condition (CTRL), exposed to lasers of 800 nm and 970 nm wavelengths and to lidocaine (Lido 100). *** $p < 0.001$, ** $p < 0.01$ (ANOVA statistical test).

laser protocols, in agreement with the lidocaine treatment. When examining the distribution of Ca inside the cells, sometimes the 970 nm led to a dispersion of the element along the cell body, while in the control cells, this element is more concentrated in a central region, likely around the nuclei as well as with the lidocaine treatment. A trend of decrement of K amount was also observed after irradiation, with the decrease being more visible after 970 nm irradiation compared to 800 nm, lidocaine treatment also resulted in a more pronounced K decrement.

S and P contents were not substantially affected by the treatments with laser or lidocaine, indicating a similar amount of the element in the control cells.

The localization of P, K and S inside the cells was not different among the conditions.

The same procedure was applied for the cells analyzed at the TwinMic beamline, focused on evaluating possible changes in Na content in cells exposed to 800 nm and 970 nm wavelength lasers (Fig. 3) and to lidocaine (Fig. 4).

The trend of the average Na and O content was shown in Fig. 5 for the four different conditions. The PBMT and lidocaine treatments were plotted separately, given that the two analyses were performed in two different experiments. The oxygen was selected as a reference element, given that a variation due to the laser or lidocaine treatment was not expected for this element. Indeed, the oxygen average counts shown in Fig. 5 confirmed comparable values between controls and treated cells. The effect of PBMT on the Na content was not evident among the conditions. However, a trend of Na decrement was observed in irradiated cells, especially in the neurons treated with the 970 nm laser. On the other hand, lidocaine treatment exhibited the opposite behavior, resulting in an increment of this element in the treated cells.

AFM microscopy was also performed on the analyzed cells to investigate possible volume and morphology changes induced by the exposure to PBMT and lidocaine. Fig. 6 depicts several neurons exposed to the different conditions, both the XRF-analyzed and illustrated in Figs. 1–5 and additional cells. No significant volume variations were observed among the different treatments. Indeed, the intensity of O, Na, P, S, K and Ca ratio to the corresponding cell volumes confirmed the same trend as the ones shown in the histograms of Figs. 2 and 5.

AFM analysis also proved that the cells' thickness and morphology were not substantially modified after the treatments (Fig. 7).

4. Discussion

Despite the worldwide employment of PBMT, the exact effect on

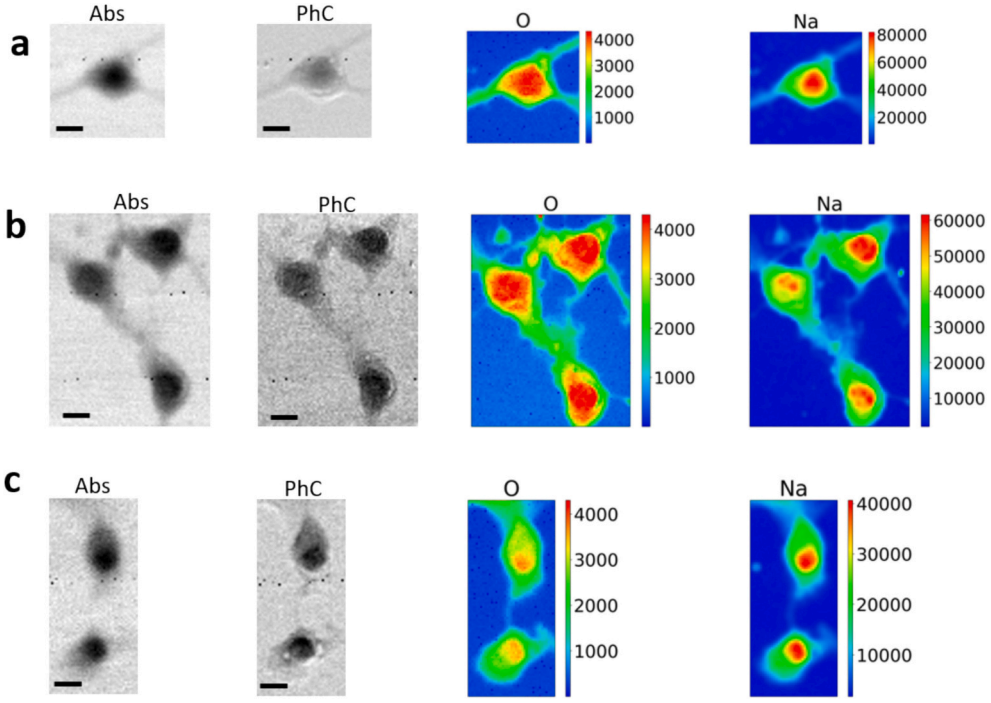

Fig. 3. Absorption (Abs) and differential phase contrast (PhC) images of control neurons (a) and neurons exposed to 800 nm laser (b) and to 970 nm laser (c), depicted together with the corresponding XRF maps of O and Na. The maps were acquired at 1.5 keV with a stepsize of 800 nm, 6 s/pixel of XRF acquisition time. Scale bars are 10 μm.

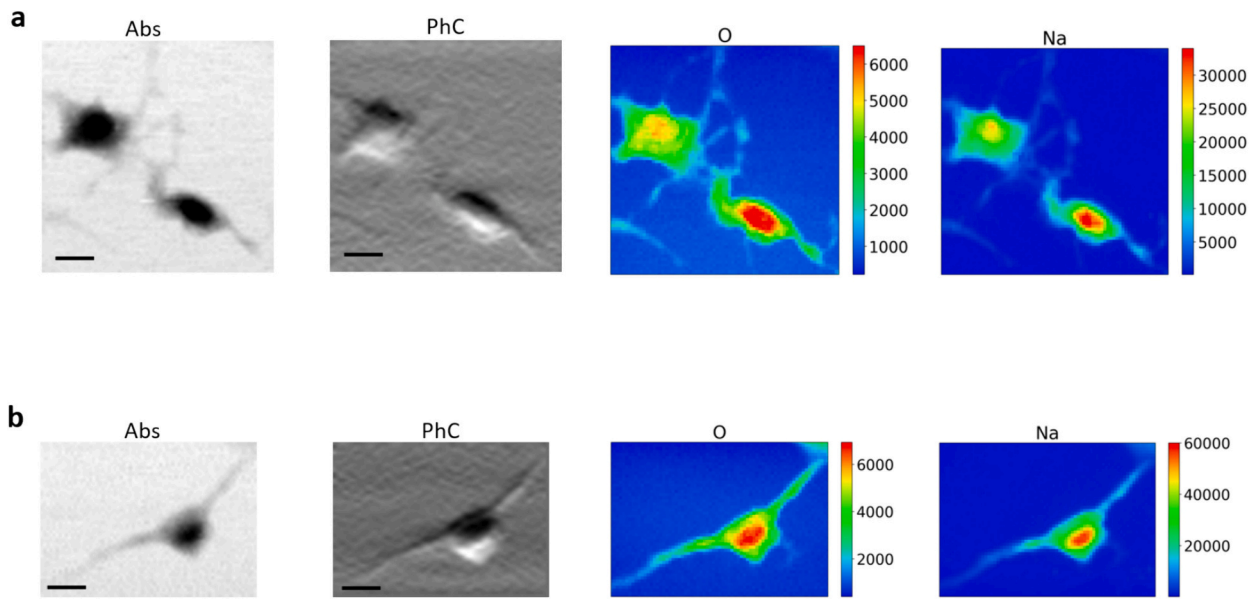

Fig. 4. Absorption (Abs) and differential phase contrast (PhC) images of control neurons (a) and neurons exposed to lidocaine (b), depicted together with the corresponding XRF maps of O and Na. The maps were acquired at 1.5 keV with a stepsize of 0.5 μm and an XRF acquisition time of 5 s/pixel. Scale bars are 10 μm.

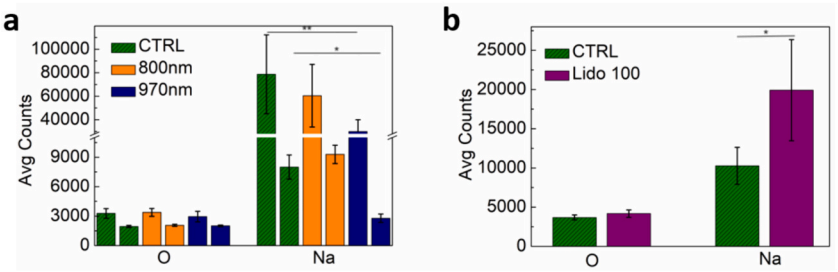

Fig. 5. Bar plots showing the average O and Na levels extracted from the O and Na maps for each mapped cell in control conditions (CTRL) and exposed to lasers of 800 nm and 970 nm wavelengths (a) and to lidocaine (Lido 100) (b). The pairs of data of panel a) refer to two different batches). ** $p < 0.001$, ** $p < 0.01$, *$p < 0.05$ (ANOVA statistical test).

neurons remains to be clarified.

Our study exploited XRF microscopy to investigate the ion content and mapping inside the cells immediately after the PBMT treatments.

A generalized reduction of calcium level was detected in the NIR-irradiated 50B11 sensory neurons. This data mirrored the results obtained with lidocaine, a well-known local anaesthetic capable of reducing calcium currents when applied to sensory neuron cells [30].

This finding suggested a potential connection between the observed data in 50B11 cells and PBMT's practical inhibitory effect on calcium levels, leading to analgesic effects.

Previous studies have demonstrated that PBMT can dynamically influence the intracellular flow of ions. In the present work, observations were conducted by fixing the cells immediately after the irradiation thus providing a static picture of the PBMT impact captured immediately after the irradiation.

The investigation into calcium levels following PBMT on cortical neurons was previously conducted by Sharma et al. [31]. Their study utilized an 830 nm laser light (25 mW/cm^2) and observed augmented calcium levels with a fluence of 3 J/cm^2 (the same as employed in the current work). Similarly, Huang et al., using an 810 nm laser, reported increased calcium levels in basal conditions but decreased excitatory in (glutamate, NMDA, or kainite) treated cortical neurons [32]. The disparities in these findings may be attributed to the distinct cell types used in the studies: cortical primary neurons in the studies by Sharma et al. [31] and Huang et al. [32] versus the sensory neuron cell line 50B11 employed in our present research. Cell-type variations could contribute to divergent responses to PBMT, highlighting the importance of considering cell-specific effects in interpreting experimental outcomes.

The data obtained with the XRF analysis allowed the display of an instant static picture of the ion content without labelling. Moreover, ions from all cellular compartments were detected, not only the free unbound ions usually labelled with the staining.

Since PBMT also influenced the activity of ion transporters, we could not exclude that a direct effect on some membrane exchangers involved in calcium transport may influence the calcium intracellular level.

In our earlier observations, pre-irradiation of 50B11 cells with NIR PBMT determined a reduction in the calcium peak following the stimulation with the TRPV1 activator, capsaicin [10]. We confirmed a similar outcome in primary DRG neurons in a previous study [9], maybe suggesting a direct effect of PBMT on this specific ion channel.

Additionally, it was demonstrated that laser light could reduce the expression of TRPV1 *in vivo* [33].

Suppression of calcium response was also detected in trigeminal neurons treated with capsaicin, as well as with TRPV4- specific activator 4-α-phorbol 12,13-didecanoate (4-αPDD), but negligible effect was observed with other TRP channels (TRPM7 and TRPM8), P2X3, native voltage-gated channels, and native P2Y, histamine, and muscarinic receptors tested [34]. Ryu et al. did not determine a reduction in the numbers of capsaicin-responders or variations in other native neuron functions, suggesting a specific effect on this channel [34].

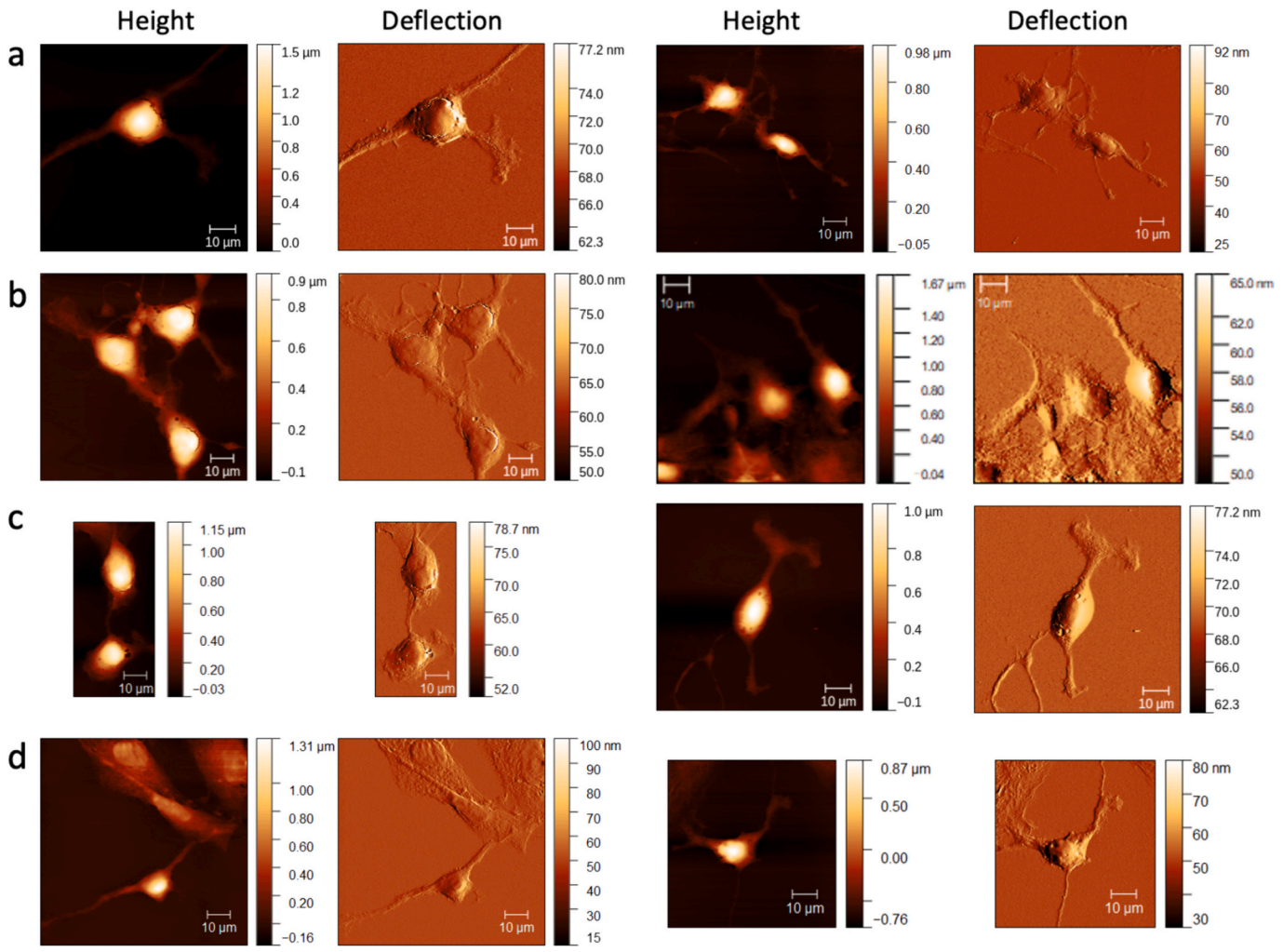

Fig. 6. AFM maps of representative control cells (a) and cells exposed to 800 nm (b) and 970 nm (c) lasers and lidocaine treatment (d). The height (left column) and amplitude/deflection (right column) signals were plotted for each map.

Five other elements of interest are O, P, S, K and Na.

The laser and drug (lidocaine) treatment did not modify the contents of O, P, and S. Indeed, by monitoring these three elements as reference elements we evaluated the corresponding variation of K, Ca and Na.

A trend of potassium and Na decrement was determined after irradiation, which was more evident with the 970 nm laser irradiation. Moreover, when the K content was normalized on the cell volume measured with AFM analysis, a more evident decrement was noted.

Lidocaine treatment resulted in a decreased level of both ions.

Although it is known that TRP channels are permeable to cations other than Ca, such as K and Na [35], an effect of PBMT on the levels of these ions has not been reported so far. We have previously demonstrated that lidocaine could interact with various cellular molecules. However, the primary target may be voltage-gated sodium channels. Lidocaine might block the channel by inhibiting Na current inside the cells. Previous studies investigated a dynamic live condition with electrophysiology methods [36,37] while our study employed a different static technique on fixed cells.

Nevertheless, we previously revealed that the fixation with paraformaldehyde was an excellent choice for analysing samples under XRF, resulting in reliable data on elements content [38].

Interestingly, no significant changes in Mg content were identified among the different conditions (not shown here).

Also, AFM microscopy shows no significant modifications neither in the volume, the thickness nor the morphology of the cells after the treatments.

To our knowledge, this study represents the first investigation into the variation of the ion content variation in neuronal cells after PBMT, revealing observable changes in their levels post-irradiation.

These findings contribute to a better understanding of the molecular impact of PBMT within neuronal cells, particularly sensory neurons, under average conditions. Such insights hold promise for promoting a broader application of PBMT.

Funding

This work was supported by the Ministry of Health, Rome - Italy, in collaboration with the Institute for Maternal and Child Health IRCCS Burlo Garofolo, Trieste - Italy (RC15/17 and RC29/23).

CRediT authorship contribution statement

Luisa Zupin: Writing – original draft, Methodology, Investigation. **Alessandra Gianoncelli:** Writing – original draft, Validation, Supervision, Investigation, Formal analysis, Data curation. **Fulvio Celsi:** Writing – review & editing, Visualization, Supervision, Conceptualization. **Valentina Bonanni:** Writing – review & editing, Methodology, Investigation, Formal analysis, Data curation. **George Kourousias:** Writing – review & editing, Validation, Methodology, Data curation. **Pietro Parisse:** Writing – review & editing, Methodology, Investigation,

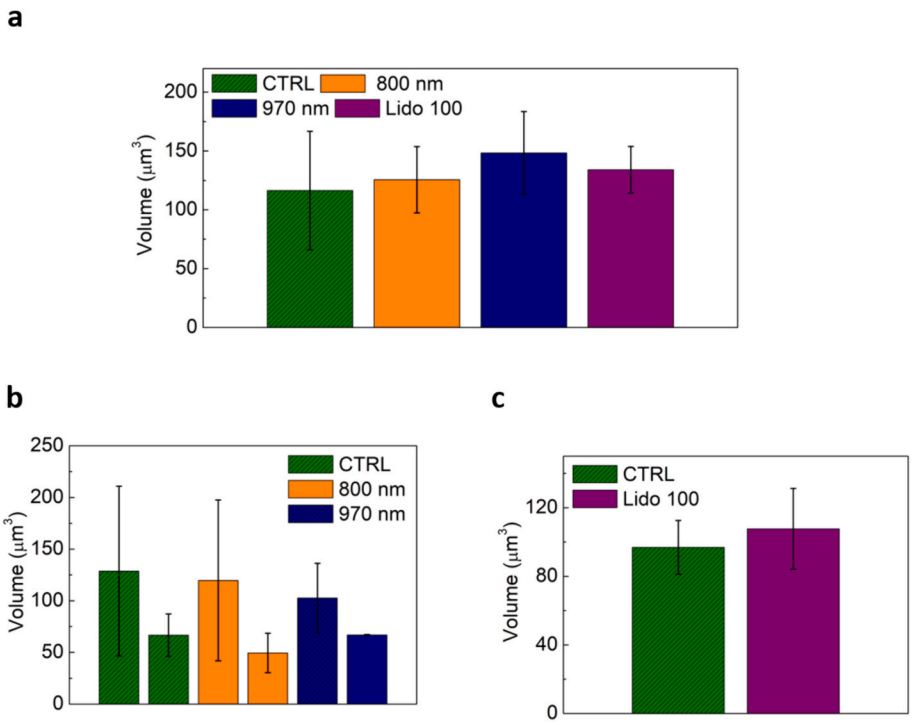

Fig. 7. Bar plots showing the average volume of the cells for control (CTRL) conditions, exposed to lasers of 800 nm and 970 nm wavelengths and to lidocaine (Lido 100) for the data collected at ID21(a) and TwinMic beamline (b and c).

Formal analysis, Data curation. **Murielle Salomé:** Writing – review & editing, Methodology, Investigation, Formal analysis, Data curation. **Sergio Crovella:** Writing – review & editing, Visualization, Supervision, Resources, Conceptualization. **Egidio Barbi:** Writing – review & editing, Visualization, Supervision, Conceptualization. **Giuseppe Ricci:** Writing – review & editing, Visualization, Supervision, Conceptualization. **Lorella Pascolo:** Writing – review & editing, Visualization, Supervision, Project administration, Methodology, Investigation, Conceptualization.

Declaration of competing interest

The authors declare that they have no known competing financial interests or personal relationships that could have appeared to influence the work reported in this paper.

Data availability

Data will be made available on request.

Acknowledgement

The 50B11 cell line was kindly provided by Prof. Ahmet Hoke (Department of Neurology and Department of Neuroscience, School of Medicine, Johns Hopkins University, Baltimore, MD) and Prof. Giovanna Gambarotta, dr. Benedetta Elena Fornasari, Dr. Sara Gnavi and prof. Stefano Geuna (Department of Clinical and Biological Sciences, and Neuroscience Institute of the Cavalieri-Ottolenghi Foundation, University of Torino, Orbassano, Italy). The authors thank Gianluca Gariani, who participated in part of the Twinmic experiment sessions; Federica Zingaro, for helping with the ID21 measurements; and Martina Bradaschia, for the English review of the manuscript.

We acknowledge Elettra Sincrotrone Trieste (Trieste, Italy) for providing access to the TwinMic beamline (experiment numbers # 20205327 and #20200146) and European Synchrotron Radiation Facility (ESRF, Grenoble, France) for providing access to the ID21 beamline (beamtime number MD1283).

The graphical abstract was created with Biorender.com

References

[1] F. Ramezani, A. Neshasteh-Riz, A. Ghadaksaz, S.M. Fazeli, A. Janzadeh, M. R. Hamblin, Mechanistic aspects of photobiomodulation therapy in the nervous system, Lasers Med. Sci. 37 (2022) 11–18, https://doi.org/10.1007/s10103-021-03277-2.

[2] M. Gobbo, F. Verzegnassi, L. Ronfani, D. Zanon, F. Melchionda, S. Bagattoni, et al., Multicenter randomized, double-blind controlled trial to evaluate the efficacy of laser therapy for the treatment of severe oral mucositis induced by chemotherapy in children: laMPO RCT, Pediatr. Blood Cancer 65 (2018) e27098, https://doi.org/10.1002/pbc.27098.

[3] E. Bardellini, F. Veneri, F. Amadori, G. Conti, A. Majorana, Photobiomodulation therapy for the management of recurrent aphthous stomatitis in children: clinical effectiveness and parental satisfaction, Med. Oral (2020) e549–e553, https://doi.org/10.4317/medoral.23573.

[4] I. Tanboga, F. Eren, B. Altınok, S. Peker, F. Ertugral, The effect of low level laser therapy on pain during dental tooth-cavity preparation in children, Eur. Arch. Paediatr. Dent. 12 (2011) 93–95, https://doi.org/10.1007/BF03262786.

[5] J.M. Bjordal, M.I. Johnson, V. Iversen, F. Aimbire, R.A.B. Lopes-Martins, Low-level laser therapy in acute pain: a systematic review of possible mechanisms of action and clinical effects in randomized placebo-controlled trials, Photomed. Laser Surg. 24 (2006) 158–168, https://doi.org/10.1089/pho.2006.24.158.

[6] R. Chow, P. Armati, E.-L. Laakso, J.M. Bjordal, G.D. Baxter, Inhibitory effects of laser irradiation on peripheral mammalian nerves and relevance to analgesic effects: a systematic review, Photomed. Laser Surg. 29 (2011) 365–381, https://doi.org/10.1089/pho.2010.2928.

[7] L.F. de Freitas, M.R. Hamblin, Proposed mechanisms of Photobiomodulation or low-level light therapy, IEEE J. Sel. Top. Quantum Electron. (2016) 22, https://doi.org/10.1109/JSTQE.2016.2561201.

[8] R.C. Hardie, Photosensitive TRPs, in: B. Nilius, V. Flockerzi (Eds.), Mammalian Transient Receptor Potential (TRP) Cation Channels Vol. 223, Springer International Publishing, Cham, 2014, pp. 795–826, https://doi.org/10.1007/978-3-319-05161-1_4.

[9] L. Zupin, G. Ottaviani, K. Rupel, M. Biasotto, S. Zacchigna, S. Crovella, et al., Analgesic effect of photobiomodulation therapy: an in vitro and in vivo study, J. Biophotonics 12 (2019) e201900043, https://doi.org/10.1002/jbio.201900043.

[10] L. Zupin, E. Barbi, R. Sagredini, G. Ottaviani, S. Crovella, F. Celsi, In vitro effects of photobiomodulation therapy on 50B11 sensory neurons: evaluation of cell metabolism, oxidative stress, mitochondrial membrane potential (MMP), and capsaicin-induced calcium flow, J. Biophotonics 14 (2021) e202000347, https://doi.org/10.1002/jbio.202000347.

[11] R.T. Chow, M.A. David, P.J. Armati, 830 nm laser irradiation induces varicosity formation, reduces mitochondrial membrane potential and blocks fast axonal flow in small and medium diameter rat dorsal root ganglion neurons: implications for

the analgesic effects of 830 nm laser, J. Peripher. Nerv. Syst. 12 (2007) 28–39, https://doi.org/10.1111/j.1529-8027.2007.00114.x.
[12] L. Zupin, S. Crovella, C. Milena, E. Barbi, F. Celsi, The mitochondrial-related effect of the 905 nm photobiomodulation therapy on 50B11 sensory neurons, J. Biophotonics 16 (2023) e202300130, https://doi.org/10.1002/jbio.202300130.
[13] K. Cheng, L.F. Martin, M.J. Slepian, A.M. Patwardhan, M.M. Ibrahim, Mechanisms and pathways of pain photobiomodulation: a narrative review, J. Pain 22 (2021) 763–777, https://doi.org/10.1016/j.jpain.2021.02.005.
[14] A. Miura, M. Kawatani, Effects of diode laser irradiation on sensory ganglion cells from the rat, Pain Res. 11 (1996) 175–183, https://doi.org/10.11154/pain.11.175.
[15] I. Golovynska, S. Golovynskyi, Y.V. Stepanov, L.I. Stepanova, J. Qu, T. Y. Ohulchanskyy, Red and near-infrared light evokes Ca2+ influx, endoplasmic reticulum release and membrane depolarization in neurons and cancer cells, J. Photochem. Photobiol. B Biol. 214 (2021) 112088, https://doi.org/10.1016/j.jphotobiol.2020.112088.
[16] W. Chen, R. Mi, N. Haughey, M. Oz, A. Höke, Immortalization and characterization of a nociceptive dorsal root ganglion sensory neuronal line, J. Peripheral Nervous Syst. 12 (2007) 121–130, https://doi.org/10.1111/j.1529-8027.2007.00131.x.
[17] R. Chow, Low level laser therapy – mechanism of action, in: Lasers in Dentistry, Wiley-Blackwell, 2015, pp. 34–39, https://doi.org/10.1002/9781118987742.ch6.
[18] B. Kaulich, A. Gianoncelli, A. Beran, D. Eichert, I. Kreft, P. Pongrac, et al., Low-energy X-ray fluorescence microscopy opening new opportunities for bio-related research, J. R. Soc. Interface (2009) 6, https://doi.org/10.1098/rsif.2009.0157.focus.
[19] R. Ortega, P. Cloetens, G. Devès, A. Carmona, S. Bohic, Iron storage within dopamine neurovesicles revealed by chemical nano-imaging, PLoS ONE 2 (2007) e925, https://doi.org/10.1371/journal.pone.0000925.
[20] S.P. Singh, K. Vogel-Mikuš, P. Vavpetič, L. Jeromel, P. Pelicon, J. Kumar, et al., Spatial X-ray fluorescence micro-imaging of minerals in grain tissues of wheat and related genotypes, Planta 240 (2014) 277–289.
[21] A. Takenori, M. Ikuhiro, U. Shogo, K. Hiroe, S. Junji, T. Yasutaka, et al., Immediate pain relief effect of low level laser therapy for sports injuries: randomized, double-blind placebo clinical trial, J. Sci. Med. Sport 19 (2016) 980–983, https://doi.org/10.1016/j.jsams.2016.03.006.
[22] M. Cotte, E. Pouyet, M. Salomé, C. Rivard, W. De Nolf, H. Castillo-Michel, et al., The ID21 X-ray and infrared microscopy beamline at the ESRF: status and recent applications to artistic materials, J. Anal. At. Spectrom. 32 (2017) 477–493, https://doi.org/10.1039/C6JA00356G.
[23] M. Salomé, M. Cotte, R. Baker, R. Barrett, N. Benseny-Cases, G. Berruyer, et al., The ID21 scanning X-ray microscope at ESRF, J. Phys. Conf. Ser. 425 (2013) 182004, https://doi.org/10.1088/1742-6596/425/18/182004.
[24] A. Gianoncelli, G. Kourousias, L. Merolle, M. Altissimo, A. Bianco, Current status of the TwinMic beamline at Elettra: a soft X-ray transmission and emission microscopy station, J. Synchrotron Radiat. 23 (2016) 1526–1537, https://doi.org/10.1107/S1600577516014405.
[25] A. Gianoncelli, G.R. Morrison, B. Kaulich, D. Bacescu, J. Kovac, Scanning transmission x-ray microscopy with a configurable detector, Appl. Phys. Lett. 89 (2006) 251117, https://doi.org/10.1063/1.2422908.
[26] A. Gianoncelli, G. Kourousias, A. Stolfa, B. Kaulich, Recent developments at the TwinMic beamline at ELETTRA: an 8 SDD detector setup for low energy X-ray fluorescence, J. Phys. Conf. Ser. 425 (2013) 182001, https://doi.org/10.1088/1742-6596/425/18/182001.
[27] V.A. Solé, E. Papillon, M. Cotte, Ph. Walter, J. Susini, A multiplatform code for the analysis of energy-dispersive X-ray fluorescence spectra, Spectrochim. Acta B At. Spectrosc. 62 (2007) 63–68, https://doi.org/10.1016/j.sab.2006.12.002.
[28] D. Nečas, P. Klapetek, Gwyddion: an open-source software for SPM data analysis, Open Phys. (2012) 10, https://doi.org/10.2478/s11534-011-0096-2.
[29] R Core Team, R: A Language and Environment for Statistical Computing, 2023.
[30] Y. Oyama, J.-I. Sadoshima, N. Tokutomi, N. Akaike, Some properties of inhibitory action of lidocaine on the Ca2+ current of single isolated frog sensory neurons, Brain Res. 442 (1988) 223–228, https://doi.org/10.1016/0006-8993(88)91507-7.
[31] S.K. Sharma, G.B. Kharkwal, M. Sajo, Y.-Y. Huang, L. De Taboada, T. McCarthy, et al., Dose response effects of 810 nm laser light on mouse primary cortical neurons, Lasers Surg. Med. 43 (2011) 851–859, https://doi.org/10.1002/lsm.21100.
[32] Y.-Y. Huang, K. Nagata, C.E. Tedford, M.R. Hamblin, Low-level laser therapy (810 nm) protects primary cortical neurons against excitotoxicity in vitro, J. Biophotonics 7 (2014) 656–664, https://doi.org/10.1002/jbio.201300125.
[33] S. Ravera, E. Colombo, C. Pasquale, S. Benedicenti, L. Solimei, A. Signore, et al., Mitochondrial bioenergetic, Photobiomodulation and trigeminal branches nerve damage, what's the connection? A review, IJMS 22 (2021) 4347, https://doi.org/10.3390/ijms22094347.
[34] J.-J. Ryu, S. Yoo, K.Y. Kim, J.-S. Park, S. Bang, S.H. Lee, et al., Laser modulation of heat and capsaicin receptor TRPV1 leads to thermal antinociception, J. Dent. Res. 89 (2010) 1455–1460, https://doi.org/10.1177/0022034510381394.
[35] G. Owsianik, K. Talavera, T. Voets, B. Nilius, Permeation and selectivity of TRP channels, Annu. Rev. Physiol. 68 (2006) 685–717, https://doi.org/10.1146/annurev.physiol.68.040204.101406.
[36] H. Dong, Y.-H. Fan, Y.-Y. Wang, W.-T. Wang, S.-J. Hu, Lidocaine suppresses subthreshold oscillations by inhibiting persistent Na+ current in injured dorsal root ganglion neurons, Physiol. Res. (2008) 639–646, https://doi.org/10.33549/physiolres.931164.
[37] M.F. Sheets, D.A. Hanck, Molecular action of lidocaine on the voltage sensors of sodium channels, J. Gen. Physiol. 121 (2003) 163–175, https://doi.org/10.1085/jgp.20028651.
[38] L. Merolle, L. Pascolo, L. Zupin, P. Parisse, V. Bonanni, G. Gariani, et al., Impact of sample preparation methods on single-cell X-ray microscopy and light elemental analysis evaluated by combined low energy X-ray fluorescence. STXM and AFM, Molecules 28 (2023) 1992, https://doi.org/10.3390/molecules28041992.